J Porous Mater (2016) 23:263–271
DOI 10.1007/s10934-015-0078-7

SO_3H-modified petroleum coke derived porous carbon as an efficient solid acid catalyst for esterification of oleic acid

Mingbo Wu[1] · Yang Wang[1] · Ding Wang[2] · Minghui Tan[1,3] · Peng Li[1] · Wenting Wu[1] · Noritatsu Tsubaki[3]

Published online: 1 October 2015

Abstract A carbon-based solid acid catalyst was simply prepared from petroleum coke by chemical activation and subsequent sulfonation. The structure–function relationships of the solid acid catalyst were investigated by regulating activation temperature. The materials were characterized by nitrogen adsorption, SEM, XRD, FT-IR and element analysis. The catalytic performances of catalysts were evaluated by the esterification of oleic acid with methanol, which is a crucial reaction in the production of biodiesel. The solid acid catalyst activated at 800 °C exhibits the most excellent catalytic activity, which is attributed to its large surface area (851 m^2/g) and high acid density (1.04 mmol/g). At the optimized conditions, high conversion (89.5 %) was achieved and no distinct activity drop was observed after five recycles. This work may offer a facile strategy to fabricate solid acid catalysts in large scale for green chemical processes.

✉ Mingbo Wu
wumb@upc.edu.cn

✉ Wenting Wu
wuwt@upc.edu.cn

✉ Noritatsu Tsubaki
tsubaki@eng.u-toyama.ac.jp

[1] State Key Laboratory of Heavy Oil Processing, China University of Petroleum, Qingdao 266580, China

[2] College of Materials Science and Engineering, University of Shanghai for Science and Technology, Shanghai 200093, China

[3] Department of Applied Chemistry, Graduate School of Engineering, University of Toyama, Gofuku 3190, Toyama 930-8555, Japan

Keywords Petroleum coke · Porous carbon · Solid acid catalyst · Biodiesel

1 Introduction

Biodiesel, as an excellent alternative to fossil fuel, has attracted great attention due to its unique properties such as low emission, non-toxicity, sustainable and environmental friendly [1, 2]. In the view of the economical production, a wide range of low-cost feedstocks including waste edible oil and animal fats have been employed to produce biodiesel [3]. However, the high amounts of free fatty acids (FFAs) in feedstocks form soap in the process of alkali-catalyzed transesterification reactions, decreasing the biodiesel yield and quality [4]. Therefore, a two-step process has been proposed to reduce the acid value of the feedstocks, which contains the acid-catalyzed pre-esterification of FFAs and the further transesterification process in the presence of base catalysts [5]. Furthermore, in order to simplify the reaction process, the esterification and transesterification can be performed simultaneously in a one-step process by using liquid acid catalysts such as H_2SO_4, HCl and H_3PO_4 [6–8]. In consideration of the drawbacks of liquid acid catalysts such as non-recyclable, costly neutralization and equipment corrosion, it is urgent to develop new acid catalysts which can eliminate the drawbacks mentioned above and realize the green synthesis.

Solid acid catalysts such as sulfonated metal oxide [9–11], sulfonated resins [12, 13], zeolite [14–16] and supported heteropoly acid catalysts [17, 18] have been proposed to replace the liquid acid catalysts. However, the shortcomings such as lack of active sites, poor stability and

high cost hinder their application. Recently, carbonhydrate-derived materials have been developed as solid acid catalyst. Hara and coworkers have proposed a series of carbon-based solid acid catalysts via carbonization of polycyclic aromatic hydrocarbon in sulfuric acid [19] or sulfonation of incompletely carbonized organic molecules [20–22]. Interestingly, such catalysts performed good catalytic performance in the esterification of acetic acid or fatty acid. Carbon-based solid acid is believed an ideal candidate to replace liquid acid catalyst due to its perfect hydrothermal stability and high catalytic performance [23–28]. However, the low surface area and poor porosity of current solid acid catalysts hinder the transportation of large molecules and reduce the catalytic activity. It is urgent to develop the porosity and specific surface area of the catalysts to further enhance the active sites accessibility [29]. In order to improve the catalytic activity, a variety of carbon materials such as graphene [30], carbon nanotube [31] and ordered mesoporous carbon [32, 33] have been used as solid acid catalyst supports on account of their superior physical structures and unique features. However, the complicated preparation processes restrict their application in biodiesel industry. It is urgent to seek a convenient and low-cost catalyst carrier. Porous carbon with simple preparation process and excellent porosity has naturally become an ideal carrier of the large-scale production of solid acid catalyst.

Petroleum coke is a by-product of the coking process in the petroleum industry and its yield increases year by year with the crude oil becoming heavier. The rational utilization of petroleum coke is an effective way to achieve high value-added of heavy oil. Petroleum coke is mainly composed of polycyclic aromatic hydrocarbons and possesses graphite layer structure. It is a promising precursor for preparing low-cost nano carbon materials such as carbon quantum dots and porous carbon due to its high carbon content [34, 35]. On the other hand, petroleum coke-based porous carbon produced by alkali activation possesses large specific surface area and relatively controllable pore size [36]. These advantages induce petroleum coke-based porous carbon become an ideal catalyst support.

Herein, we explored the feasibility of developing low cost solid acid catalysts based on porous carbon derived from petroleum coke and explored their catalytic performance in the esterification of oleic acid. Petroleum coke derived porous carbons with different structures were produced just by regulating the activation temperature. The physical and chemical characteristics of porous carbons and solid acid catalysts were systematically characterized and the effects of the sulfonation process on the catalyst supports were clarified.

2 Experimental

2.1 Prepartion of solid acid catalyst

Potassium hydroxide (KOH), oleic acid (>99 % purity), methanol (99.8 % purity, moisture content <0.05 %), and nitric acid (HNO_3) were purchased from Sinopharm Chemical Reagent Co., Ltd. Methyl heptadecanoate (GC standard) was purchased from Adirich. Sulfuric acid (98 wt% H_2SO_4) was purchased from Laiyang Fine Chemical Corp. The petroleum coke with 0.32 wt% of ash, 0.48 wt% of moisture and 15.36 wt% of volatile from Sinopec Qilu Branch was used as raw material.

The preparation of carbon-based solid acid catalyst involved two steps. The first step was the synthesis of petroleum coke based porous carbon. The original petroleum coke powder was physically mixed with KOH (99 %) at a mass ratio of 1:3, then carbonized at 500 °C in nitrogen for 1 h, and activated at different temperatures, i.e. 600, 700, 800 and 900 °C in nitrogen for 2 h. Finally, the samples were washed with HNO_3 aqueous solution and distilled water until the pH value of the filtrate became neutral and dried at 60 °C for 8 h. The samples synthesized at different activation temperatures were denoted as PC-600, PC-700, PC-800 and PC-900, respectively. The second step was the sulfonation of porous carbon with concentrated H_2SO_4. 1 g porous carbon was added into 100 mL concentrated H_2SO_4 at 120 °C under magnetic stirring. After 10 h, the resultant material was diluted with hot distilled water, filtered, washed thoroughly until the pH value of the filtrate became neutral and dried at 60 °C for 8 h. The as-made solid acid catalyst were denoted as PC-600-SO_3H, PC-700-SO_3H, PC-800-SO_3H and PC-900-SO_3H.

2.2 Samples characterization

The yield of porous carbon was calculated according to the following formula Yield (%) = $(m_{pc}/m_p) \times 100$ %, where m_{pc} and m_p are the weights of the porous carbon and the original petroleum coke, respectively. The powder X-ray diffraction (XRD) patterns of the catalysts were characterized with a PANalytica X'Pert PRO X-ray diffractometer using Cu K_α radiation. Fourier transform infrared (FT-IR) were measured with a NEXUS FT-IR spectrometer in the range of 400–4000 cm^{-1}. The surface area and pore size distribution of the porous carbons and solid acid catalysts were measured with a Micromeritics ASAP 2020 M instrument. All samples were degassed at 200 °C prior to nitrogen adsorption. Pore size and pore volume were calculated according to the Barrett–Joyner–Halenda (BJH) formula. C, H, S analyses of the petroleum coke and solid

acid catalysts were carried out by combustion in a Elementar Vario EL III elemental analyzer equipped with a TCD detector. The metal components of the petroleum coke and solid acid catalysts were measured by a Analytik Jena contraa 700 atomic-absorption spectrometer. The total acid density of the catalysts were determined by acid–base titration. 50 mg catalyst was added to NaOH solution (25 mL, 0.01 M). After being stirred for 24 h, the solid was separated from the solution by filtration. Then 5 mL filtrate was taken out for titration with HCl aqueous solution (0.1 M). The total acid density of the catalyst was estimated by calculating the amount of consumed NaOH.

2.3 Catalytic testing

The catalytic performance of obtained solid acid catalysts was carried out in the esterification of oleic acid and methanol in a flask equipped with a reflux condenser, an oil bath and a magnetic stirrer. Typically, 0.1 g solid acid catalyst was added to 2.8 g oleic acid and 4 mL methanol at 80 °C. After given reaction times, the catalysts were separated from the solution by centrifugation, and the product was separated with a rotary evaporator and diluted with n-hexane. The yield of methyl oleate was analyzed by gas chromatography (PerkinElmer Clarus 580 series) equipped with a flame ionization detector (FID) and a HP-5 capillary column, and methyl heptadecanoate was used as the internal standard. The conversion of oleic acid was calculated as Con (%) = $m_{(MO)} \times 100$ %/m, where Con (%) is the conversion of oleic acid, $m_{(MO)}$ is the amount of methyl oleate, and m is the amount of initial oleic acid. The cycle performance of the catalyst was investigated by repeating five cycles of the esterification of oleic acid at the same reaction conditions. The used catalyst was separated from reaction system by centrifugation and washed repeatedly with ethanol and distilled water after each experiment. The washed catalyst was vacuum dried at 65 °C.

3 Results and discussion

3.1 Effect of preparation conditions on the structure of petroleum coke derived catalyst

The chemical components of the petroleum coke were analyzed by element analyses, and the weight percents of C, H, N and S are 89.45, 4.32, 1.58 and 0.32 %, respectively. Atomic-absorption spectroscopy provides metal contents (0.12 % of Fe^{3+} and 0.08 % of Mn^{2+}). The element contents of the petroleum coke derived porous carbon are given in Table 1. It is worth noting that S and N contents of the porous carbon are negligible, which is attributed to the release of N and S in the form of NO_x and SO_x during the KOH activation process of petroleum coke [45]. Furthermore, the heavy metals in solid acid catalysts can be completely removed by concentrated sulfuric acid, guaranteeing the eco-friendly concept in the catalytic applications.

The surface functional groups of porous carbons derived from petroleum coke and the corresponding solid acid catalysts were characterized by FT-IR spectra. As shown in Fig. 1, the petroleum coke derived porous carbons contain both aromatic and aliphatic hydrocarbons. The vibration bands at 2890 and 850 cm^{-1} are ascribed to the C–H in aliphatic hydrocarbons and aromatic hydrocarbons, respectively. The broad and intense bands at 1520 cm^{-1} is assigned to the aromatic like C=C stretching mode in graphite-like polyaromatic materials. In addition, the characteristic peaks of C–H stretching mode of PC-900 weaken gradually, indicating the dehydrogenation of petroleum coke over a certain range of temperature [37]. As illustrated in Table 1, the variation of carbon content of porous carbon also can be revealed by the element analysis. The FT-IR spectra of the solid acid catalysts are shown in Fig. 1b. The vibration bands at 1010 and 1040 cm^{-1} are attributed to S=O symmetric stretching and asymmetric stretching, which confirm the successful attachment of $–SO_3H$ onto the carbon matrix [38]. The peak at 1710 cm^{-1} is assigned to C=O stretching vibration. Also, the peak at 3400 cm^{-1} is due to the –OH stretching mode of –COOH, and phenolic –OH groups are significantly enhanced, which represent the introduction of –OH and –COOH by sulfonation. Furthermore, after sulfonation of carbon precursors, the peaks of C–H stretching mode in aromatic (850 cm^{-1}) and aliphatic (2890 cm^{-1}) hydrocarbons disappear, as well as the peaks at 1520 cm^{-1} due to the C=C stretching mode become weaker, indicate that the sulfonated steps not only introduce $–SO_3H$ onto the carbon framework, but also change the structure of the raw carbon materials. The results are in agreement with previous study that an aromatic and unsaturated C=C at the edge or defect sites of carbon sheets can be attacked to form a hydroxyl group, and continue to be broken up to form carboxylic acid group under strong oxidizing conditions [39].

Figure 2 is XRD patterns of petroleum coke derived porous carbons and solid acid catalysts. All of the XRD patterns have two diffraction peaks at around $2\theta = 20°$ and 45°, corresponding to the graphitic (002) and (101) planes, respectively. These diffraction patterns are typical amorphous carbon consisting of polycyclic aromatic carbon sheets oriented in a random fashion [40]. With the activation temperature increase, the diffraction peaks ($2\theta = 15–35°$) assigned to amorphous carbon decrease and diffraction peaks ($2\theta = 45°$) assigned to graphite-like carbon structure become weaker, suggesting the

Table 1 Chemical properties of the porous carbon and the corresponding catalysts

Sample	Element content (wt%)				$-SO_3H$ density (mmol/g)[a]	Total acid density (mmol H^+/g)[b]
	C	H	O	S		
PC-600	85.81	0.68	13.51	–	–	–
PC-600-SO_3H	83.87	0.70	13.90	1.53	0.48	0.69
PC-700	85.18	2.89	11.93	–	–	–
PC-700-SO_3H	83.02	2.90	12.10	1.98	0.62	0.80
PC-800	84.98	4.56	10.46	–	–	–
PC-800-SO_3H	81.62	4.60	10.52	3.26	1.04	1.21
PC-900	83.55	4.16	12.29	–	–	–
PC-900-SO_3H	80.29	4.37	13.14	2.20	0.69	0.90

[a] Measured by elemental analysis

[b] Measured by acid–base titration

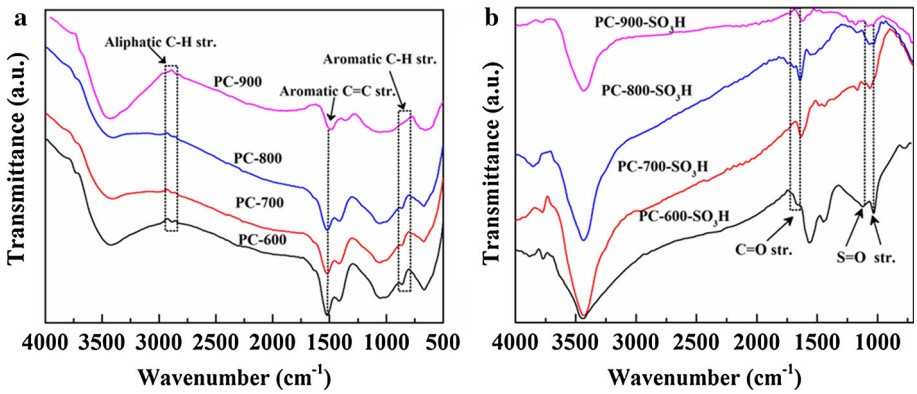

Fig. 1 FT-IR spectra of **a** petroleum coke derived porous carbons and **b** carbon-based solid acid catalysts

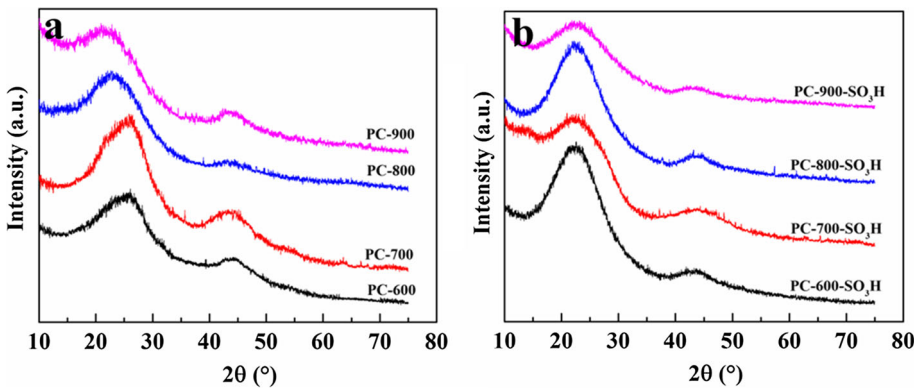

Fig. 2 X-ray diffraction patterns of **a** petroleum coke derived porous carbons and **b** carbon-based solid acid catalysts

destruction of graphite layer structure at high activation temperature. The d_{002} as shown in Table 2 were calculated by using the Scherer equations. The lattice spacing d_{002} increases from 0.337 nm for PC-600 to 0.341 nm for PC-700, 0.382 nm for PC-800 and 0.395 nm for PC-900, which indicate the increasing distance of the graphite layer. All XRD patterns reveal that petroleum coke activated at higher temperature yields porous carbon with more disorder orientation. These features make H_2SO_4 contact with carbon sheets easier, which is consistent with the increasing sulfur content in Table 1 [41]. It is noted that PC-900 seems to be an exception due to its low specific surface area, which hinders H_2SO_4 contact with the defects of the porous carbon. The amorphous carbon structure was preserved after sulfonation, while the (002) peak strengthened, which assigned to H_2SO_4 destroy the

Table 2 Textural properties of porous carbons and catalysts and the catalytic performance of the catalysts

Sample	S_{BET} (m^2/g)[a]	D (nm)[b]	V (cm^3/g)[c]	d_{002} (Å)[d]	Yield (%)[e]	Con (%)[f]
PC-600	864	3.12	0.05	3.37	65	–
PC-600-SO_3H	886	2.87	0.04	3.96	–	73.9
PC-700	1063	3.15	0.11	3.41	59	–
PC-700-SO_3H	1103	2.32	0.06	3.85	–	70.4
PC-800	750	5.45	0.31	3.82	51	–
PC-800-SO_3H	851	3.52	0.14	3.93	–	89.5
PC-900-3	577	5.93	0.44	3.95	42	–
PC-900-SO_3H	660	3.85	0.22	4.13	–	82.0

Reaction conditions: 2.8 g oleic acid, 4 mL methanol, 0.1 g catalyst, and 80 °C for 8 h

[a] Specific surface area estimated by the BET method

[b] Average pore diameter estimated by BJH formula

[c] Pore volume estimated by BJH formula

[d] *d*-spacing of 002 diffraction

[e] Yield of the porous carbon

[f] Conversion of oleic acid

stacking of carbon sheets, and this phenomenon is in accordance with the increasing lattice spacing of the sulfanated porous carbon compared to the carbon supports as shown in Table 2 [42, 43].

The catalytic activity of solid acid catalysts depends on the surface texture and porosity of the catalyst support [44]. The structure characteristics of the porous carbon obtained at different preparation conditions are shown in Table 2. At different activation temperatures, petroleum coke was successfully activated to make porous carbon with high surface area and large pore volume, which are both important to the ideal catalyst support. The N_2 adsorption–desorption isotherms and pore size distribution curves of the porous carbon in Fig. 3 indicate that the porous carbon activated at 600 °C belongs to Type I isotherm, which represents the microporous character. The isotherm still keep as type I, while the quantity of nitrogen adsorption increases, which indicates that more proportion of micropores was generated when the activation temperature went up to 700 °C. The nitrogen adsorption–desorption isotherms of PC-800 exhibits an obvious H_4 type hysteresis loop, signifying the presence of mesopores, which caused the decreasing specific surface area. The porous carbon produced at 900 °C possesses the lowest specific surface area due to the worst destruction of carbon matrix at high temperature. At the same time, the deep activation at high temperature further enlarge the pore size of the porous carbon (5.94 nm), which is in accordance with our previous work [45]. Figure 4 gives the schematic of carbon-based solid acid catalysts. The preparation of petroleum coke derived porous carbon contains carbonization and further activation processes. In the initial phase, the active agent reacts with oxygen-containing functional groups on the surface of petroleum coke. With the temperature increases, the active agent begins to react with the methyl and methylene groups of petroleum coke, and lots of micropores (0–2 nm) develop in this process. The size of the pores formed formerly can be enlarged when the temperature further increases. This phenomenon can be attributed to the formation of K^+, which can react with petroleum coke intensively. The reduction of the yield of porous carbon versus enhanced activation

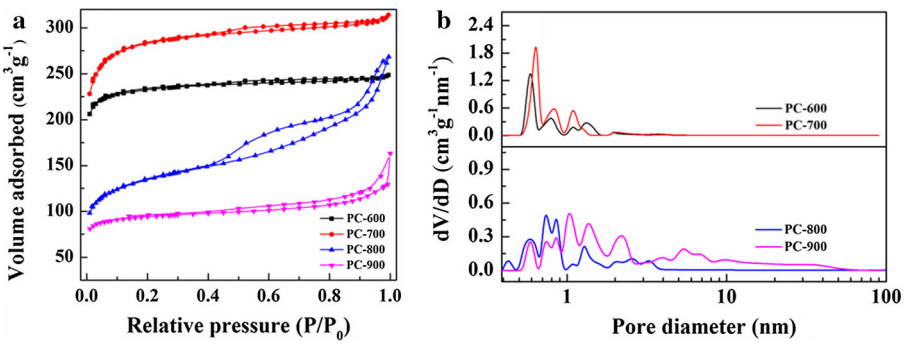

Fig. 3 N_2 adsorption–desorption isotherms (**a**) and pore size distribution (**b**) of petroleum coke derived porous carbons

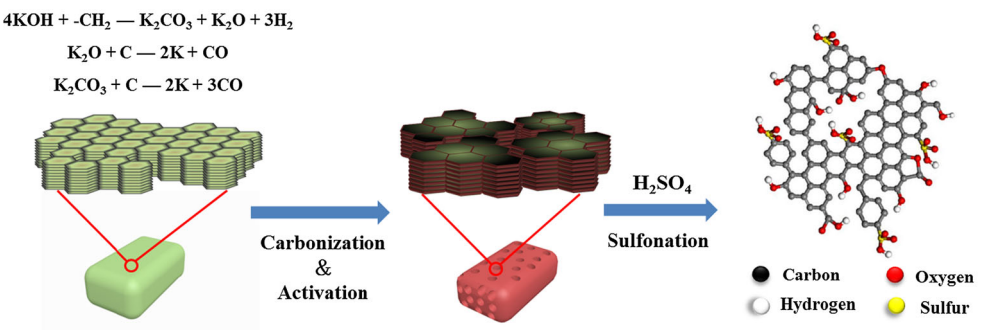

Fig. 4 Preparation schematic of carbon-based solid acid catalysts

temperature (see Table 2) also reveals that further activation take place.

Figure 5a, b show the N_2 adsorption–desorption isotherms of solid acid catalysts. It can be observed that the sulfonation process has a great impact on the pore structure of porous carbon. The BET surface area of the porous carbon increases in different extent after modification with sulfonic acid due to the dehydrogenation reaction on the defects of the carbon sheets during the sulfonation process, which can produce a large number of micropores. Foo et al. [42] speculated that the functional groups presented on the surface of porous carbon could be converted to porous domains during the sulfonation with H_2SO_4, which results in a slightly increase surface area of solid acid catalysts. It also can be identified as a sign of the introduction of $–SO_3H$ to the carbon matrix due to the $–SO_3H$ can occupy a part of channel space. The catalysts show obvious variation in architectural features compared to the initial porous carbons. This phenomenon is attributed to the formation of large pore volume and pore size, as well as thin wall of the hole in the process of activation, so as to the poor stability of the structure of the porous carbon under severe sulfonation conditions. Even though the outstanding change in physical architecture, the catalysts possess large pore size and high density of $–SO_3H$, which is favorable to the catalytic performance.

Figure 6 shows the SEM images of PC-800 and PC-800-SO_3H. The inset in Fig. 6a is the SEM image of starting petroleum coke. The petroleum coke shows smooth surface, while the porous carbon exhibits porous structure. Besides micro-sized pores, PC-800 possesses a lot of mesopores and macro-pores, which are helpful to the following sulfonation process. This morphology characteristics accelerate the sufonation of the exposed defect sites, thus form larger pores as illustrated in Fig. 6b, indicating promising structure characteristics as catalyst for the biomass conversion.

The acid densities of solid acid catalysts were determined by acid–base titration and elemental analysis (Table 1). FT-IR spectra indicate that the solid acid catalysts contain $–SO_3H$ groups, which are strong acid sites, and two kinds of weak acid sites, i.e. –OH and –COOH, although only strong acid sites determine the catalytic performance in the esterification of oleic acid with methanol [46]. Generally, the acid–base titration method can calculate the total acid density, however, cannot distinguish weak and strong acid sites. Due to the negligible amount of elemental S in porous carbon, the $–SO_3H$ density has been roughly estimated through the total S content of the sulfonated porous carbon based on the assumption that all S are in the form of $–SO_3H$ [38, 47]. It has been demonstrated that the introduction of $–SO_3H$ to the surface of the carbon supports is associated with the reaction between H_2SO_4 and –OH groups [33, 42, 48, 49], and the porous carbon activated by KOH possess large number of oxygen-containing groups, which is favorable to the

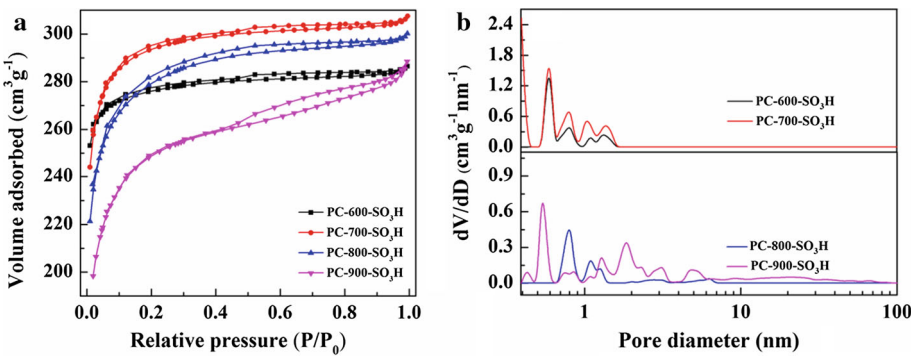

Fig. 5 N_2 adsorption–desorption isotherms (**a**) and pore size distribution (**b**) of carbon-based solid acid catalysts

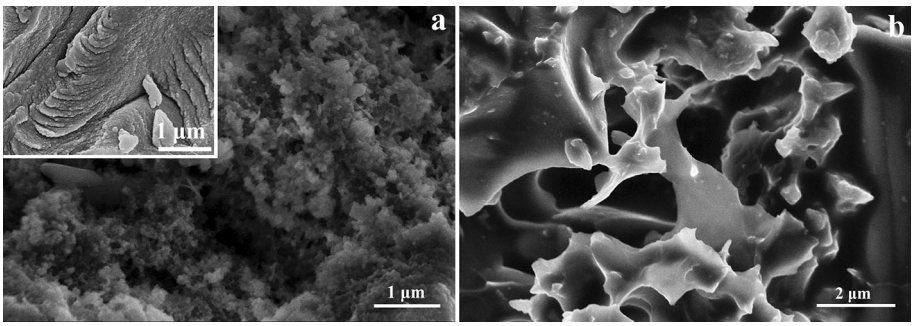

Fig. 6 SEM images of **a** petroleum coke derived porous carbon PC-800 (*inset* is the corresponding petroleum coke) and **b** carbon-based solid acid catalyst PC-800-SO_3H

modification of –SO_3H. On the other hand, the density of –SO_3H is also related to the pore structure and skeleton of the porous carbon [37]. The porous carbon produced at high temperature can form a lot of defect sites and carbon sheet edges, which can provide ideal position for the introduction of strong acid groups –SO_3H [50]. The low specific surface area of PC-900 will decrease the locations of sulfonation taking place, which lead to the drop in –SO_3H intensity. So the introduction of –SO_3H is largely controlled by the surface chemical property and physical structure of the catalyst supports.

3.2 Catalytic performance of solid acid catalyst

The catalytic activities of the solid acid catalysts were evaluated by the esterification of oleic acid and methanol, which is one of the key reaction in the production of biodiesel. The mechanism for esterification has been reported previously [51]. Traditionally, the carbocation generated from the interaction of carbonyl oxygen of oleic acid with the acidic site of the catalyst can be attacked by methanol.

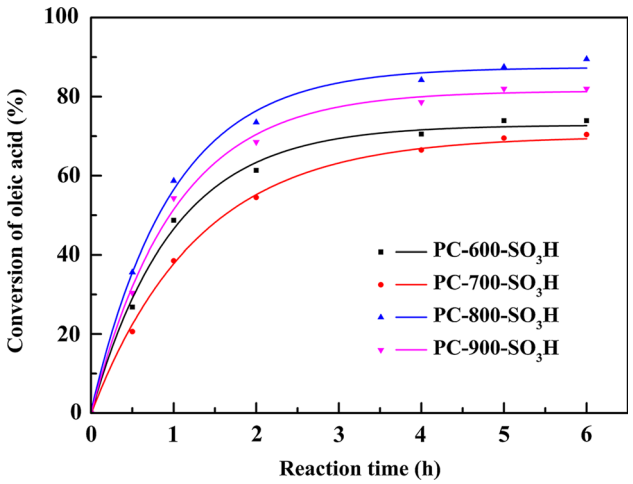

Fig. 7 Esterification of oleic acid with methanol over petroleum coke-based solid acid catalysts. Reaction conditions: 2.8 g oleic acid, 4 mL methanol, 0.1 g solid catalyst, and 80 °C

And this nucleophilic attack can produce tetrahedral intermediate, which will eliminate H_2O to form methyl oleate. The active site can return back to the original form. Figure 7 shows the catalytic performances of the carbon-based solid acid catalysts. Obviously, all catalysts reach the maximum conversion after 6 h. PC-800-SO_3H shows the best catalytic performance with the oleic acid conversion higher than 89.5 %, which is comparable with other carbon-based solid acid catalysts reported in the literatures (see Table 3) [38, 41, 52, 53]. The superior catalytic performance of solid acid catalysts can be attributed to the synergistic effect of abundant strong acid and large pore size. Compared to PC-600-SO_3H, PC-700-SO_3H abnormally shows poorer catalytic performance in spite of its larger surface area and more strong acid density, which is due to a lot of narrow and long pores formed at 700 °C. This narrow pores hinder the access of long-chain carboxylic oleic acid into the active sites. PC-900-SO_3H with good active site accessibility also exhibits low catalytic activity compared to PC-800-3-SO_3H, indicating that high density of active sites also play an important role in the catalytic reaction. In conclusion, large pore structure and high strong acid density are vital factors in the conversion of biomass, especially to the long-chain molecule. Due to the analogous mechanism between esterification and trans-esterification, the authors believe that this low-cost and easily prepared solid acid catalyst also has potential application in the trans-esterification process as reported by C. Poonjarernsilp et al. [51]. In our group, the carbon-based catalysts driving biomass conversion are being investigated [54, 55].

3.3 Reusability of solid acid catalyst

The reusability of catalysts is a vital property in practical application. As shown in Fig. 8, the catalytic activity of PC-800-SO_3H gradually decreases, but the decrease of the conversion is not obvious. The conversion of oleic acid is more than 85 % after five cycles, which demonstrated that –SO_3H modified porous carbon was a stable carbon-based

Table 3 Comparison of the esterification of oleic acid with methanol catalyzed by PC-800-SO_3H and other catalysts reported in the literatures

Catalyst	S_{BET} (m^2/g)	D (nm)	–SO_3H density (mmol/g)	Con (%)
PC-800-SO_3H	851	3.52	1.04	89.5
SC-Al-900[a]	1118	8.16	1.86	77.7 [38]
Ca-648, 0.5-Sul-423,15[b]	–	–	1.06	90.5 [41]
OMC-H_2O_2-SO_3H[c]	475	3.50	1.86	86.0 [52]
OMC-150-SO_3H[d]	741	4.20	1.70	73.6 [53]

[a] Reaction conditions: 1 g oleic acid, 8 mL methanol, 20 mg catalyst, and 65 °C for 1.25 h

[b] Reaction conditions: 2.8 g oleic acid, 4 mL methanol, 80 °C, 0.14 g catalyst and 5 h

[c] Reaction conditions: 14 g oleic acid, 40 mL methanol, 80 °C, 0.1 g catalyst and 5 h

[d] Reaction conditions: 1.4 g oleic acid, 2 mL methanol, 80 °C, 0.05 g catalyst and 10 h

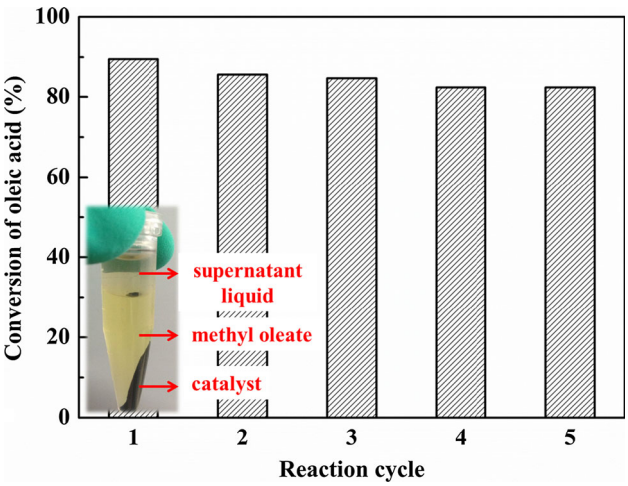

Fig. 8 Recyclability of PC-800-SO_3H for the esterification of oleic acid. Reaction conditions: 2.8 g oleic acid, 4 mL methanol, 0.1 g solid catalyst, and 80 °C for 6 h. *Inset* Photograph of the centrifugalized product

solid acid catalyst. To clarify the deactivation of the catalyst, the strong acid density of the reused catalyst after five cycles were determined by sulfur element analysis, the strong acid density of PC-800-SO_3H was reduced from 1.04 mmol H^+/g to 0.8 mmol H^+/g. The leaching of polycyclic aromatic hydrocarbons containing –SO_3H is responsible to the reduction of strong acid sites and the deactivation of the catalyst in addition to the –SO_3H groups fall into the reaction system. Furthermore, in order to test whether –SO_3H leach out into methyl oleat, the centrifugalized methyl oleat (see inset in Fig. 8) was washed with water to extract –SO_3H possibly leached from the catalyst. $BaCl_2$ precipitation test demonstrated that no –SO_3H exists in the washed water. The leached out –SO_3H could exist in the supernatant liquid due to the hydrophilicity of –SO_3H, which ensure no sulfur in final methyl oleat. Although the obvious reduction happens on strong acid sites, the remaining active sites also guarantee an excellent conversion of oleic acid.

4 Conclusions

In summary, a carbon-based solid acid catalyst was prepared from petroleum coke by KOH activation and subsequent sulfonation. The catalyst exhibits remarkable catalytic performance in the esterification of oleic acid with methanol due to the multifuntionalized groups (–SO_3H, –COOH, –OH), large surface area and high strong acid density. At the optimized conditions, 89.5 % conversion of the oleic acid to methyl oleate was achieved by the porous carbon activated at 800 °C. More importantly, PC-800-SO_3H can be easily separated from reaction system via filtration after catalytic reaction and recycled without obvious loss of deactivation. Consequently, the catalyst shows great prospect of industrial application due to its superior catalytic performance, simple preparation process and low-cost raw material. The petroleum coke-based solid acid catalysts will provide a green strategy for the production of biodiesel.

Acknowledgments This work is supported by the National Natural Science Foundation of China (Nos. 51172285, 51372277, 51402192); the Fundamental Research Funds for the Central Universities (No.15CX08005A); State Key Laboratory of Heavy Oil Processing (SKLHOP201503).

References

1. A.F. Lee, J.A. Bennett, J.C. Manayil, K. Wilson, Chem. Soc. Rev. **43**, 7887 (2014)
2. F. Su, Y. Guo, Green Chem. **16**, 2934 (2014)
3. A. Birla, B. Singh, S.N. Upadhyay, Y.C. Sharma, Bioresour. Technol. **106**, 95 (2012)
4. J.Y. Park, D.K. Kim, J.S. Lee, Bioresour. Technol. **101**, 62 (2010)
5. G. Corro, N. Tellez, E. Ayala, A. Marinez-Ayala, Fuel **89**, 2815 (2010)
6. S. Yan, S.O. Salley, K.Y.S. Ng, Appl. Catal. A Gen. **353**, 203 (2009)
7. G. Chen, B.S. Fang, Bioresour. Technol. **102**, 2635 (2011)
8. F. Guo, Z. Fang, X.F. Tian, Y.D. Long, L.Q. Jiang, Bioresour. Technol. **102**, 6469 (2011)
9. K. Arata, Green Chem. **11**, 1719 (2009)
10. B.M. Reddy, M.K. Patil, Chem. Rev. **109**, 2185 (2009)

11. J.A. Melero, J. Iglesias, G. Morales, Green Chem. **11**, 1285 (2009)
12. X.M. Zhang, Y.P. Zhao, S.T. Xu, Y. Yang, J. Liu, Y.X. Wei, Q.H. Yang, Nature Commun. **5**, 3170 (2014)
13. E. Andrijanto, E.A. Dawson, D.R. Brown, Appl. Catal. B Environ. **115**, 261 (2012)
14. D.H. Zuo, J. Lane, D. Culy, M. Schultz, A. Pullar, M. Waxman, Appl. Catal. B Environ. **129**, 342 (2013)
15. C. Pirez, J.M. Caderon, J.P. Dacquin, A.F. Lee, K. Wilson, ACS Catal. **2**, 1607 (2012)
16. F. Hoffmann, M. Cornelius, J. Morell, M. Froeba, Angew. Chem. Int. Ed. **45**, 3216 (2006)
17. M.G. Kulkarni, R. Gopinath, L.C. Meher, A.K. Dalai, Green Chem. **8**, 1056 (2006)
18. K. Srilatha, T. Issariyakul, N. Lingaiah, P.S.S. Prasad, J. Kozinski, A.K. Dalai, Energy Fuels **24**, 4748 (2010)
19. M. Hara, T. Yoshida, A. Takagaki, T. Takata, J.N. Kondo, S. Hayashi, K. Domen, Angew. Chem. Int. Ed. **43**, 2955 (2004)
20. S. Suganuma, K. Nakajima, M. Kitano, D. Yamaguchi, H. Kato, S. Hayashi, M. Hara, J. Am. Chem. Soc. **130**, 12787 (2008)
21. M. Okamura, A. Takagaki, M. Toda, J.N. Kondo, K. Domen, T. Tatsumi, M. Hara, S. Hayashi, Chem. Mater. **18**, 3039 (2006)
22. M. Toda, A. Takagaki, M. Okamura, J.N. Kondo, S. Hayashi, K. Domen, M. Hara, Nature **438**, 178 (2005)
23. D.S. Su, S. Perathoner, G. Centi, Chem. Rev. **113**, 5782 (2013)
24. M.M. Titirici, R.J. White, N. Brun, V.L. Budarin, D.S. Su, F. del Monte, J.H. Clark, M.J. MacLachlan, Chem. Soc. Rev. **44**, 250 (2015)
25. L. Wang, F.S. Xiao, Green Chem. **17**, 24 (2015)
26. E. Lam, J.H.T. Luong, ACS Catal. **4**, 3393 (2014)
27. B.B. Chang, Y.L. Tian, W.W. Shi, J.Y. Liu, F.N. Xi, X.P. Dong, J. Porous Mater. **20**, 1423 (2013)
28. B.B. Chang, Y.C. Li, Y.Z. Guo, H. Yin, S.R. Zhang, B.C. Yang, J. Porous Mater. **22**, 629 (2015)
29. B. Hu, C.R. Xiong, K. Tao, S.H. Zhou, J. Porous Mater. **22**, 613 (2015)
30. F.J. Liu, J. Sun, L.F. Zhu, X.J. Meng, C.Z. Qi, F.S. Xiao, J. Mater. Chem. **22**, 5495 (2012)
31. B.L. Oliveira, V.T. da Silva, Catal. Today **234**, 257 (2014)
32. Z.H. Gao, S.K. Tang, X.L. Cui, S.J. Tian, M.H. Zhang, Fuel **140**, 669 (2015)
33. J.F. Pang, A.Q. Wang, M.Y. Zheng, T. Zhang, Chem. Commun. **46**, 6935 (2010)
34. M.B. Wu, Y.Y. Ren, N. Guo, S.B. Li, X.Y. Sun, M.H. Tan, D. Wang, J.T. Zheng, N. Tsubaki, Mater. Lett. **82**, 124 (2012)
35. M.B. Wu, Y. Wang, W.T. Wu, C. Hu, X.N. Wang, J.T. Zheng, Z.T. Li, B. Jiang, J.S. Qiu, Carbon **78**, 480 (2014)
36. Y. Shi, J.W. Chen, J. Chen, R.A. Macleod, M. Malac, Appl. Catal. A Gen. **441**, 99 (2012)
37. M.H. Zhang, A.X. Sun, Y.L. Meng, L.T. Wang, H.X. Jiang, G.M. Li, Microporous Mesoporous Mater. **204**, 210 (2015)
38. L. Geng, G. Yu, Y. Wang, Y.X. Zhu, Appl. Catal. A Gen. **427**, 137 (2012)
39. J. Zhang, H.L. Zou, Q. Qing, Y.L. Yang, Q.W. Li, Z.F. Liu, X.Y. Guo, Z.L. Du, J. Phys. Chem. B **107**, 3712 (2003)
40. N. Tsubouchi, C.B. Xu, Y. Ohtsuka, Energy Fuels **17**, 1119 (2003)
41. W.Y. Lou, Q. Guo, W.J. Chen, M.H. Zong, H. Wu, T.J. Smith, Chemsuschem **5**, 1533 (2012)
42. G.S. Foo, C. Sievers, Chemsuschem **8**, 534 (2015)
43. Y.Z. Hong, Z.Y. Wang, X.B. Jin, Sci. Rep. **3**, 3439 (2013)
44. L. Wang, J. Zhang, S. Yang, Q. Sun, L.F. Zhu, Q.M. Wu, H.Y. Zhang, X.J. Meng, F.S. Xiao, J. Mater. Chem. A **1**, 9422 (2013)
45. M.B. Wu, Q.F. Zha, J.S. Qiu, X. Han, Y.S. Guo, Z.F. Li, A.J. Yuan, X. Sun, Fuel **84**, 1992 (2005)
46. L. Geng, Y. Wang, G. Yu, Y.X. Zhu, Catal. Commun. **13**, 26 (2011)
47. K. Nakajima, M. Hara, ACS Catal. **2**, 1296 (2012)
48. B.B. Chang, J. Fu, Y.L. Tian, X.P. Dong, RSC Adv. **3**, 1987 (2013)
49. D. Nandan, P. Sreenivasulu, S.K. Saxena, N. Viswanadham, Chem. Commun. **47**, 11537 (2011)
50. C.L. Su, M. Acik, K. Takai, J. Lu, S.J. Hao, Y. Zheng, P.P. Wu, Q.L. Bao, T. Enoki, Y.J. Chabal, K.P. Loh, Nature Commun. **3**, 1298 (2012)
51. C. Poonjarernsilp, N. Sano, H. Tamon, Appl. Catal. A Gen. **497**, 145 (2015)
52. B.B. Chang, J. Fu, Y.L. Tian, X.P. Dong, J. Phys. Chem. C **117**, 6252 (2013)
53. R. Liu, X.Q. Wang, X. Zhao, P.Y. Feng, Carbon **46**, 1664 (2008)
54. D. Wang, G.H. Yang, Q.X. Ma, M.B. Wu, Y.S. Tan, Y. Yoneyama, N. Tsubaki, ACS Catal. **2**, 1958 (2012)
55. D. Wang, W.Q. Niu, M.H. Tan, M.B. Wu, X.J. Zheng, Y.P. Li, N. Tsubaki, Chemsuschem **7**, 1398 (2014)